Cellulose (2021) 28:1387–1403
https://doi.org/10.1007/s10570-020-03618-4

ORIGINAL RESEARCH

Particle size distributions for cellulose nanocrystals measured by atomic force microscopy: an interlaboratory comparison

Michael Bushell · Juris Meija · Maohui Chen · Warren Batchelor · Christine Browne · Jae-Young Cho · Charles A. Clifford · Zeinab Al-Rekabi · Oriana M. Vanderfleet · Emily D. Cranston · Malcolm Lawn · Victoria A. Coleman · Gustav Nyström · Mario Arcari · Raffaele Mezzenga · Byong Chon Park · ChaeHo Shin · Lingling Ren · Tianjia Bu · Tsuguyuki Saito · Yuto Kaku · Ryan Wagner · Linda J. Johnston

Received: 4 September 2020 / Accepted: 10 December 2020 / Published online: 6 January 2021

Abstract Particle size measurements of cellulose nanocrystals (CNCs) are challenging due to their broad size distribution, irregular shape and propensity to agglomerate. Particle size is one of the key parameters that must be measured for quality control purposes and to differentiate materials with different properties. We report the results of an interlaboratory comparison (ILC) which examined atomic force microscopy (AFM) data acquisition and data analysis protocols. Samples of CNCs deposited on poly-L-lysine coated mica were prepared in the pilot laboratory and sent to 10 participating laboratories including academic, government and industrial organizations with varying levels of experience with imaging CNCs. The participant data sets indicated that the central

Supplementary information The online version of this article (https://doi.org/10.1007/s10570-020-03618-4) contains supplementary material, which is available to authorized users.

M. Bushell · J. Meija · M. Chen · L. J. Johnston (✉)
National Research Council Canada, Ottawa, ON K1A 0R6, Canada
e-mail: Linda.Johnston@nrc-cnrc.gc.ca

W. Batchelor · C. Browne
Department of Chemical Engineering, Bioresource Processing Research Institute of Australia, Monash University, Clayton, VIC 3800, Australia

J.-Y. Cho
Nanotechnology Research Centre, National Research Council Canada, Edmonton, AB T6G 2M9, Canada

C. A. Clifford · Z. Al-Rekabi
National Physical Laboratory, Teddington, Middlesex TW11 0LW, UK

O. M. Vanderfleet · E. D. Cranston
Department of Chemical Engineering, McMaster University, Hamilton, ON L8S 4L8, Canada

E. D. Cranston
Departments of Wood Science and Chemical and Biological Engineering, The University of British Columbia, Vancouver, BC V6T 1Z4, Canada

M. Lawn · V. A. Coleman
National Measurement Institute Australia, Lindfield, NSW 2070, Australia

G. Nyström
Empa–Swiss Federal Laboratories for Materials Science and Technology, Überlandstrasse 129, 8600 Dübendorf, Switzerland

G. Nyström · M. Arcari · R. Mezzenga
Department of Health Sciences and Technology, ETH Zurich, Schmelzbergstrasse 9, 8092 Zurich, Switzerland

B. C. Park · C. Shin
Center for Nanocharacterization, Korean Institute of Standards and Science, Daejeon 34113, Republic of Korea

location, width and asymmetry varied considerably for both length and height distributions. To deal with this variability we used a skew normal distribution to model the data from each laboratory and to obtain the consensus distribution that describes the CNC particle size. The skew normal distribution has 3 parameters: a central location (mean), distribution width (standard deviation) and asymmetry (shape) factor. This approach gave consensus distributions with mean, standard deviation and asymmetry factor of 94.9 nm, 37.3 nm and 6.0 for length and 3.4 nm, 1.2 nm and 2.8 for height, respectively. The use of multiple probes and/or deterioration of the probe with increased use are significant contributing factors to the variability in mean length between laboratories. There is less variability in height across participating laboratories and tests of applied imaging force indicate that it is possible to image without significant compression of the CNCs. The number of CNCs necessary to obtain a reliable data set depends on the probes and operating conditions, but with careful control of various parameters analysis of 250 and 300 CNCs should provide consistent data sets for height and length, respectively for one sample. Comparison of AFM with transmission electron microscopy (TEM) data obtained in the same ILC demonstrated excellent agreement between measured lengths for the 2 methods. By contrast AFM height was approximately one half the TEM width, a result that indicates the presence of a significant number of laterally agglomerated particles, consistent with literature data.

Graphic abstract

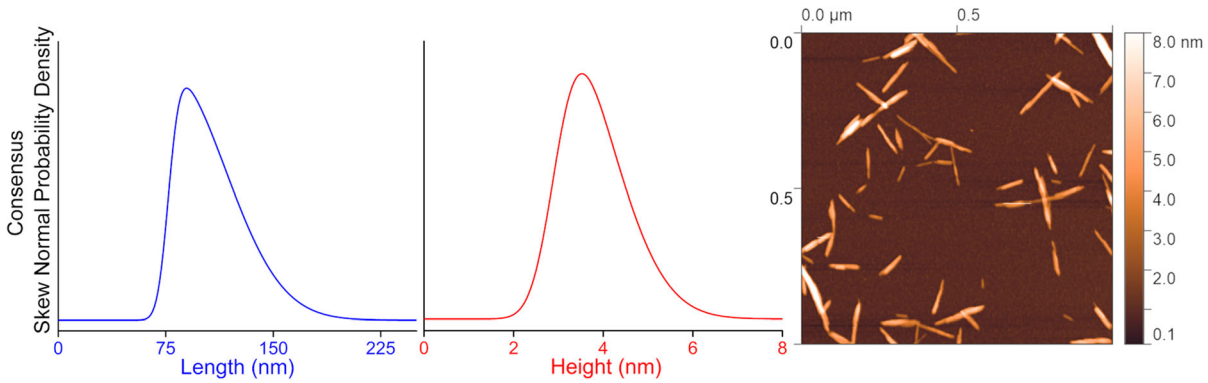

L. Ren · T. Bu
National Institute of Metrology,
Chaoyang District, Beijing 100029, China

T. Saito · Y. Kaku
Department of Biomaterial Sciences, Graduate School of Agricultural and Life Sciences, The University of Tokyo,
1-1-1 Yayoi, Bunkyo-ku, Tokyo 113-8657, Japan

R. Wagner
Asylum Research, Santa Barbara, CA 93117, USA

Keywords Cellulose nanocrystals · Atomic force microscopy · Particle size distributions · Interlaboratory comparison

Introduction

Cellulose nanocrystals (CNCs) are a family of emerging nanomaterials that are attracting considerable attention for applications such as additives for nanocomposites, thin films, rheology modifiers, and biomedical products (Shatkin et al. 2014; Grishkewich et al. 2017; Mondal 2017; Mokhena and John 2020). CNCs are derived from cellulose, the world's most abundant biopolymer, and are produced from a number of biomass sources including wood pulp, plants, bacterial cellulose and marine organisms (Klemm et al. 2011; Moon et al. 2011). Their large scale production from a renewable resource, novel properties, and anticipated minimal toxicity make them an attractive candidate for applications, some of which are nearing commercial success. CNCs are nanorods with a typical aspect ratio of $\geq$ 15 (for wood pulp CNCs), high crystalline cellulose content and mechanical strength, and a low coefficient of thermal expansion (Klemm et al. 2011; Moon et al. 2011; Reid et al. 2017). Most CNC production methods generate negatively charged groups on the particle surface, providing colloidally stable dispersions and sites for further functionalization (Mondal 2017). Development of applications for this novel nanomaterial requires reliable characterization protocols that can be used for quality control purposes and to ensure reproducible production of the material from different biomass sources. Validated characterization methods and reference materials are equally important for studies aimed at ensuring the safe use of these materials (Shatkin and Kim 2015).

Particle size and shape, crystallinity and surface functional group identity and density are some of the key properties that must be assessed for CNCs. Particle size distributions are of particular interest, not only for quality control during production, but also because the CNC size distribution and polydispersity have large effects on sample viscosity and CNC self-assembly processes (Schütz et al. 2018). The irregular rod-shaped structure of CNCs coupled with their broad size distributions and strong tendency to agglomerate make particle size measurements by microscopy a challenging endeavour (Jakubek et al. 2018). This is in contrast to well-behaved, approximately spherical gold and silica nanoparticles that typically have monomodal size distributions. Both transmission electron microscopy (TEM) and atomic force microscopy (AFM) have been widely employed for particle size measurements by the CNC community, although a standard approach for sample preparation, imaging and image analysis is currently lacking (Moon et al. 2014; Kaushik et al. 2015; Foster et al. 2018; Stinson-Bagby et al. 2018; Ogawa and Putaux 2019).

Atomic force microscopy has some advantages over TEM for measuring CNC size distributions. The contrast between particles and background is generally higher for AFM and the sample preparation is simpler than for TEM which typically requires ultra-high vacuum and a second staining step that may introduce additional particle agglomeration (Kaushik et al. 2015). Furthermore, AFM is compatible with measurement of the mechanical properties of the material which is advantageous for some studies (Lahiji et al. 2010). These advantages are somewhat offset by the generally longer data acquisition times for AFM, although this limitation can in principle be addressed by state-of-the-art fast scan instruments. Another factor to take into account is that AFM and TEM provide two different measures of the particle cross-section; TEM provides particle width while AFM is typically used to measure particle height. Very few studies have used both AFM and TEM to characterize the same CNC samples (Elazzouzi-Hafraoui et al. 2008; Postek et al. 2011; Brito et al. 2012; Brinkmann et al. 2016; Meng et al. 2017; Korolovych et al. 2018) and there are few direct comparisons of the 2 methods. Note that one expects the 2 methods to give comparable cross-section values if the particles are symmetric and agglomeration or surface-induced deformation (Mattos et al. 2019) is minimized. However, the AFM height and TEM width will be different if the particles are asymmetric or laterally agglomerated, as reported previously (Brinkmann et al. 2016; Jakubek et al. 2018). Assuming that the 2 methods measure a similar length, different cross-sectional dimensions will lead to different aspect ratios, an important consideration for some applications (Schütz et al. 2018).

There are relatively few examples of AFM protocol validation using round robin or ILC comparisons.

Notable examples include the characterization of a bimodal silica reference material and 2 ILCs that examined gold, silver, silica and polystyrene nanoparticles (Meli et al. 2012; Kestens et al. 2016; Lin et al. 2019). In 2 of these studies AFM and electron microscopy (EM) were used by multiple labs and the results were compared to those obtained using other particle sizing methods. Two other studies evaluated methods of assessing uncertainty in AFM measurements and compared AFM and EM measurements of spherical nanoparticles in the same laboratory (Delvallée et al. 2015; Delvallee et al. 2016). By contrast many studies have explored the validation of TEM protocols for various nanomaterials, including titanium dioxide, gold nanorods and carbon black, which are all more challenging samples than spherical silica or metal nanomaterials (Grulke et al. 2017, 2018a, b).

We report here the AFM results from an interlaboratory comparison (ILC) conducted under the auspices of the Versailles Project on Advanced Materials and Standards (VAMAS) Technical Working Area 34 (Nanoparticle Populations). The ILC objective was to assess the performance of protocols for AFM and TEM imaging and subsequent particle size analysis of CNCs. The ILC used a National Research Council of Canada (NRC) reference material, CNCD-1 (http://www.nrc.ca/crm), with samples prepared by the pilot laboratory in order to reduce the impact of sample preparation and focus specifically on instrument operating conditions and image analysis. TEM results have been published separately (Meija et al. 2020); the combined AFM and TEM results will provide the pre-normative data necessary for an ISO/TC 229 (Nanotechnologies) technical specification (TS 23,151) on microscopy particle size measurements for CNCs. CNC particle size measurements were provided by 10 participating laboratories. The data were modelled as skew normal distributions which have 3 parameters: the mean (a measure of central tendency), the standard deviation (a measure of the spread of the distribution) and a shape factor that accounts for variable degrees of asymmetry in individual data sets. Final consensus values were obtained by modelling the variation between laboratories using a skew normal distribution and overlap index plots are used to assess the similarity of data sets.

Experimental

Sample preparation

An NRC certified cellulose nanocrystal reference material, CNCD-1, was used for sample preparation (http://www.nrc.ca/crm). This material was produced by hydrolysis of softwood pulp, followed by neutralization with NaOH, yielding CNCs with sulfate half ester groups on their surface, and has been thoroughly characterized (Jakubek et al. 2018; Johnston et al. 2018). Dry CNC was dispersed by probe sonication to give a 2% by mass suspension, as outlined in the papers describing the characterization of CNCD-1; full details are provided in the Experimental Section of the Supplementary Information. Samples for ILC participants were prepared on several days over a 3 week period to ensure that each laboratory received the sample at a pre-arranged (convenient) date. One sample from each day was checked via AFM imaging prior to sending the samples to participants. Samples were attached to adhesive pads in the sample boxes and sealed in a nitrogen glove box prior to shipping. Internal testing showed no observable change in AFM image quality over 5 weeks.

Participating laboratories

The participating institutions were from Asia, Australia, Europe and North America and included 3 universities, 6 government laboratories, 4 of which are national metrology institutes, and 1 industrial laboratory. Not all laboratories had prior experience with imaging CNCs. Two samples of CNCs on poly-L-lysine (PLL, Sigma-Aldrich) coated mica were sent to each participant; the second sample was a backup in case of issues with sample 1. Participants were asked to image the samples within 2 weeks of receipt.

Image acquisition protocol

Participants were requested to dimensionally calibrate the AFM prior to imaging according to the manufacturer's recommendations or the laboratory's standard practice, unless the instrument use and calibration records indicated that the previous calibration was still valid. Intermittent contact mode imaging was recommended. Several large scale images were to be recorded to verify sample quality before recording a

series of 1 μm × 1 μm (or smaller) images with a minimum resolution of 512 × 512 pixels (to ensure a pixel size of ≈2 nm) and scan rates < 1 Hz. Participants were instructed to verify that the applied imaging force was the minimum that allowed for stable imaging by measuring the CNC height as a function of applied imaging force (as controlled by the cantilever amplitude feedback setpoint) for one or more images (Jakubek et al. 2018). Probe selection (resonance frequency, spring constant, tip geometry and dimensions) was left to the participant's discretion and the protocol noted that multiple probes would typically be required. Images were to be acquired from multiple regions close to the centre of the substrate, avoiding areas previously imaged; a sufficient number of images to analyze a minimum of 500 single particles was requested.

Image analysis protocol and data analysis

The protocol provided an example of image analysis using Gwyddion (free, open-source software, version 2.52 recommended); however, participants had an option to use the software of their choice as long as the same guidelines for image flattening and particle selection were used. The Gwyddion protocol draws line profiles through the long axis of the particle for all individual CNCs in each image. The line profiles are used to determine the height and length for each particle; see Fig. S1 and further details on selection of individual CNCs in the Supplementary Information (Jakubek et al. 2018). This procedure reduces data analysis time relative to one-at-a-time manual measurement of CNC profiles to extract length and height data. The significant level of aggregation makes it impractical to use an automated analysis approach. Participants were requested to return the original image files, the corresponding files with analyzed particles numbered and the completed Excel template. The Excel template contained length, height and aspect ratio data, image acquisition and analysis parameters and histograms for each measurand.

Data sets from each laboratory were reviewed and descriptive statistics were evaluated using Origin Pro 2019. Origin was also used to test for fits of the data to various distribution models and for statistical comparison of data sets using the non-parametric two-sample Kolmogorov–Smirnov (K–S) test (significance level 0.05). More complex data analysis and visualization was performed in R (a free, open source software environment for statistical computing and graphics) whereas hierarchical skew normal model fitting was performed using Markov Chain Monte Carlo methods using STAN (a probabilistic programming language for statistical inference written in C + +). The overlap index used to compare particle size distributions was calculated by integrating the areas under curves using the standard numerical facilities of R. In all cases fitting was done using the full data set, not the binned data shown in the histograms.

Results and discussion

Tests of image analysis protocols

The first phase of the ILC focused on testing the previously reported Gwyddion image analysis method developed for characterization of the NRC certified reference material, CNCD-1 (Jakubek et al. 2018). Six AFM images were sent to 3 participants for analysis using Gwyddion. The selected images were a subset of those collected for 1 sample of CNCD-1 by the pilot laboratory. The returned data sets and the original CNCD-1 data for the same images from 2 analysts are summarized in Table S1 and as box plots in Fig. S2. Despite differences of up to a factor of 2 in the number of individual CNCs analyzed (which varies from 87 to 198), the data sets give similar mean and median values for both length and height. The standard deviation of the length distribution varies by approximately 20% across the 4 data sets. Two sample K–S analysis of the data sets indicated that only 1 of the 6 possible pairs had significantly different distributions for length and none were significantly different for height. Based on these results, it was concluded that the Gwyddion protocol was adequate for analysis of CNC size, and thus was used for the second phase of the ILC.

Initial survey of AFM results

Results for AFM imaging and analysis of CNCs were submitted from 10 participating laboratories; each participant submitted raw data (images), processed images with analyzed particles numbered, tables of length and height for each particle analyzed,

histograms and a table summarizing instrument operating parameters, and data processing and analysis. The instruments, operating parameters, dimensional calibration information, AFM probe properties, analysis software and number of particles analyzed for each laboratory are summarized in Table S2. Instruments from 4 manufacturers were used, all were operated in intermittent contact mode and calibration information was provided (Table S2). One laboratory used a semi-automated data acquisition mode. With one exception 1 μm × 1 μm images with 512 × 512 pixels were analyzed; one laboratory (A5) imaged at higher resolution with 1024 × 1024 pixels. The number of CNCs analyzed was lower than the recommended value of 500 for 4 labs, with the remaining laboratories analyzing between 500 and 620 CNCs. Time required was reported as the limiting factor for the number of CNCs imaged. Probes were purchased from a range of manufacturers and had nominal spring constants between 0.4 and 42 N/m, resonance frequencies from 70 to 400 kHz and nominal probe radii between 2 and 10 nm. Multiple probes were used by 6 laboratories. Images were analyzed using the Gwyddion protocol provided to the participants with 2 exceptions (Table S2); the latter laboratories used Nanoscope and open source software (FiberApp) (Usov and Mezzenga 2015). One laboratory used a Matlab routine for height and length measurements from the CNC profiles generated in Gwyddion. Tests of the applied imaging force were provided by 7 laboratories; a representative example is shown in Fig. S3. The use of instruments from 4 different manufacturers and AFM probes with a wide range of properties effectively covers the typical range of conditions that are likely to be employed by many laboratories.

Representative images from 2 laboratories are shown in Fig. 1 to illustrate the image quality and the typical level of CNC dispersion. Note the significant number of touching or clustered particles in the images, despite the relatively low CNC density and efforts to optimize the dispersion. Box plots of the length and height data for each laboratory are shown in Fig. 2 and individual histograms for length, height and aspect ratio for each laboratory are provided in Fig. S4, S5 and S6, respectively. In several cases examination of the box plots indicated that apparent outliers may have been errors in reported data; this was verified by examining the processed image files and consulting with the participant on the removal or correction of the data point(s).

The results in Fig. 2, S4 and S5 show qualitatively that the maximum position, shape, width and asymmetry of the distributions vary considerably for the 10 laboratories. This variability is also illustrated by the plots shown in Fig. S7, which provide a simple graphical display of the range that covers 10–90% of the data for each laboratory. The variability between laboratories is larger for length than for height. Challenges with selection of individual particles are likely to contribute to this variability. For example, the features marked with arrows in Fig. 1 and Fig. S1 indicate multiple aggregated particles; however, some of these features might be analyzed as individual particles in some cases, depending on the analyst bias and the image quality. In some cases the individual particles have slightly tapered ends which may also make the analysis more challenging. Note that the ten data sets contain variable numbers of particles with length > 200 nm (Fig. 2), although these do not have a large impact on either mean or median.

Effect of AFM probes and number of analyzed particles

Six laboratories used multiple AFM probes for imaging, although one did not record the probe used for specific images. In order to evaluate the effect of using multiple probes, presumably with different spring constants and tip radii, we initially examined the data obtained with multiple AFM probes in 4 laboratories. Two sample K–S tests were used to evaluate whether the data sets obtained with different probes in each laboratory were the same or different without an assumption of the distribution model. The results for the comparison of length and height data obtained with various tips, including the number of CNCs per data set, are summarized in Tables S3 and S4. This comparison indicates that the use of multiple AFM probes had relatively minor effects on the measured height for a specific laboratory since the K–S tests showed no significant difference in data sets. By contrast, 7 of the 19 possible pairs of data sets for length have distributions that are significantly different using the K–S test. This observation could be due to tip-particle convolution effects, the magnitude of which will change with the tip radius and geometry. However, it should be noted that the nominal tip radius

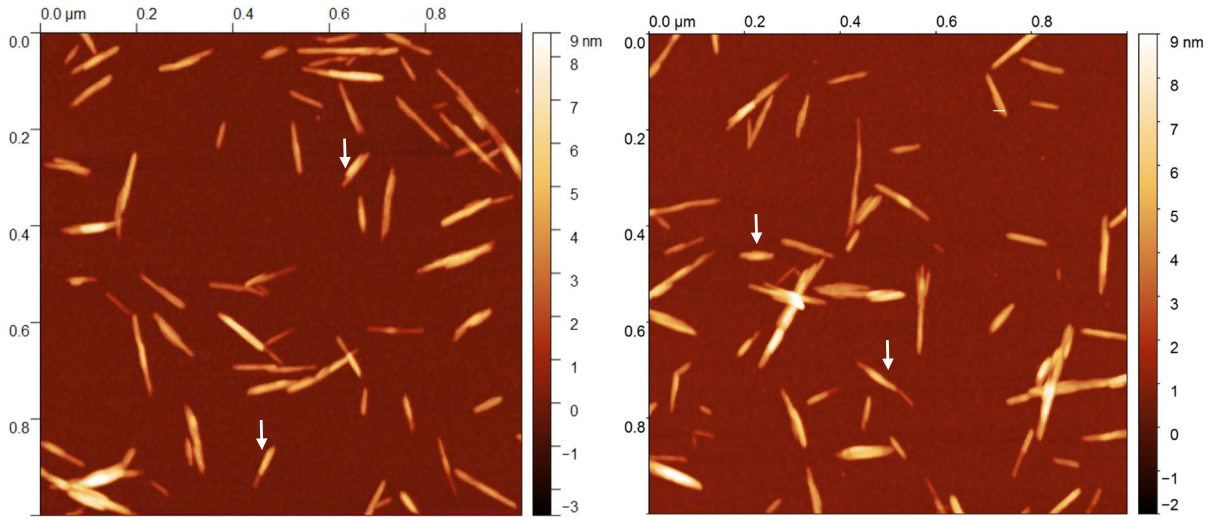

Fig. 1 Representative AFM images from labs A4 (left) and A7 (right). The arrows show features that may be more than one CNC

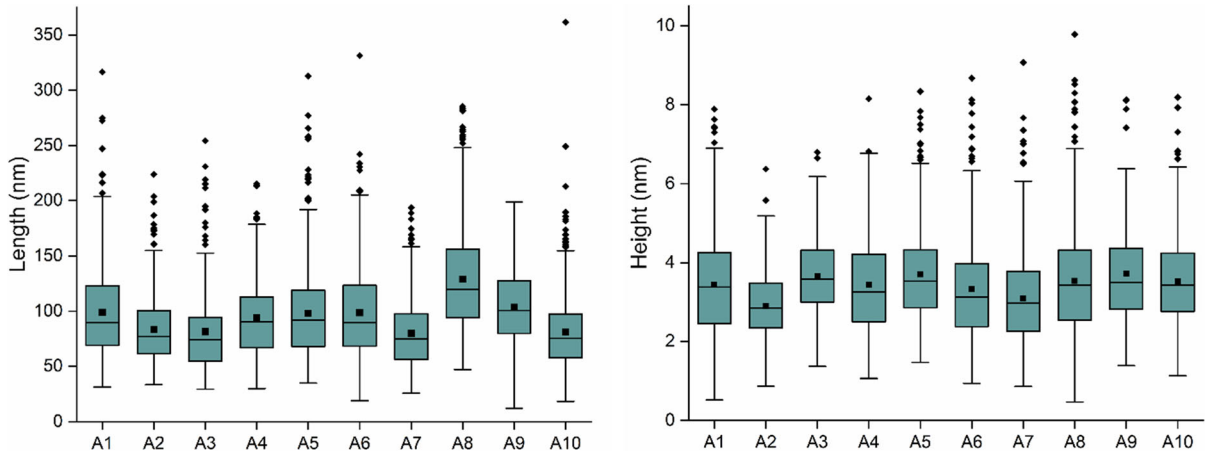

Fig. 2 Box plots for length and height data from each participating laboratory. The bottom and top of the colored boxes represent the 25th and 75th percentiles; the mean and median are shown as a square and solid line, respectively; the vertical bars are 1.5 times the interquartile range, with points that fall outside this range shown as filled diamonds

is similar (Table S1, 7–10 nm) for the probes used in the 4 laboratories and it is likely that the tip may change relatively rapidly during initial imaging due to either contamination or wear. An alternative possibility is that the relatively limited statistics for some of the probe-specific data sets ($N = 60$ to $N = 221$) contribute to variations in length with different probes. However, this does not appear to be the case for laboratory A7 (Table S4) since only 20% of the length pairs are different, even though the number of CNCs analyzed is lower than in the data sets for the other 3 laboratories.

The variability in particle size as a function of the number of probes used and the number of particles analyzed was examined in more detail by plotting the cumulative mean length and height for each AFM probe as a function of the number of particles analyzed. Representative results are shown in Fig. 3 for length data from 4 laboratories; length and height plots for all laboratories are shown in Fig. S8–11. There are several interesting observations that arise from this data. First, the mean length for different probes used by a single laboratory varies significantly in some cases (probe 2 for A1 and probe 1 for A2,

Fig. 3); in other cases probes behave similarly (probes 1 and 3 for A1 and probes 2 and 3 for A2). The mean length systematically decreases as more CNCs are imaged for some probes (probe 2 for A1 and probe 1 for A2). The second observation from Fig. 3 and Fig. S9 is that the use of a single probe leads to a systematic increase over time of up to 15 nm in the measured length for some data sets (A5 and A9) as more images are collected. This is indicative of wear or contamination of the probe with longer use. However, data sets A3 and A10 showed more random variations in mean as the number of images increased and the fluctuations covered a smaller range ($\sim$ 6 nm and $\sim$ 3 nm, respectively, Fig. 3 and S9). Both these laboratories used a low spring constant probe (nominally $<$ 1.5 N/m) which may contribute to less wear and contamination of the probe.

The variability in height data when multiple probes are used by a single laboratory is less pronounced than that observed for length, although the trends are qualitatively similar (Fig. S10). This is consistent with the results of the K–S tests shown in Table S3, which indicate that the distributions for height are not significantly different. The data sets that were obtained with a single probe are consistent with systematic evolution of the probe properties (Fig. S11) with height values changing by 0.25–0.4 nm during image collection. However, as noted above, this does not typically lead to data sets that are significantly different based on a K–S test.

The cumulative plots shown in Fig. 3 and S8–S11 provide interesting information on differences between probes and evolution of the probe as a function of the number of images. The variations between probes may reflect differences in spring constant and tip size and shape. In principle this could be addressed by calibration of the cantilever spring constant and tip geometry and radius for each probe. Since the tip is likely to change due to either contamination or wear, in situ assessment with an internal calibration standard may be necessary to assess the tip size. Nevertheless, this would be a time-consuming task that is incompatible with routine measurements. The evolution of probe properties as a function of the number of images is particularly clear in some cases where a single probe was used to collect all images; some probes used to collect smaller data sets also show this effect. This makes it difficult to provide guidelines on the number of probes that are required, which will be a function of the probe and instrument operating conditions. In fact, monitoring CNC size on a per image basis during data collection may be necessary, at least until the laboratory has established appropriate conditions for minimizing and identifying changes in probe properties. The results also indicate that use of more compliant cantilevers for soft tapping avoids some of the issues of probe evolution during imaging. The variation between probes and the change in probe properties make it challenging to identify an optimal number of CNCs to achieve a statistically reliable result. However, the results indicate that with careful control of imaging conditions and attention to potential deterioration of the tip, it should be possible to achieve a repeatable result with fewer than 500 CNCs, approximately 300 CNCs for length or 200–250 CNCs if only height is required. Previously reported AFM studies provide different values for the number of particles required to generate statistically meaningful data sets. Most of these studies imaged spherical nanoparticles with relatively narrow size distributions and, therefore, may not be relevant to polydisperse rod-shaped CNCs (Meli et al. 2012; Delvallee et al. 2016; Lin et al. 2019).

Particle size distributions

Statistical modeling of interlaboratory results requires the selection of an appropriate probability function to describe the data. To date most CNC microscopy size measurements have reported data as histograms with the calculated mean and the standard deviation as a measure of the distribution width (Beck-Candanedo et al. 2005), making the implicit assumption that the distributions follow a normal model. In several cases, CNC size data have been fitted to a lognormal distribution, which is frequently recommended for nanoparticle size distributions (Kiss et al. 1999; Elazzouzi-Hafraoui et al. 2008; Postek et al. 2011; Usov et al. 2015; Schütz et al. 2018). Recent ILC studies of other nano-objects have tested a variety of distribution models in an attempt to better represent the overall central location and breadth/shape of the distributions. These studies have investigated TEM data for particles with irregular shapes and high polydispersity such as gold nanorods, titanium dioxide and carbon black as well as electron microscopy and ICP-MS data for spherical particles (Montoro Bustos

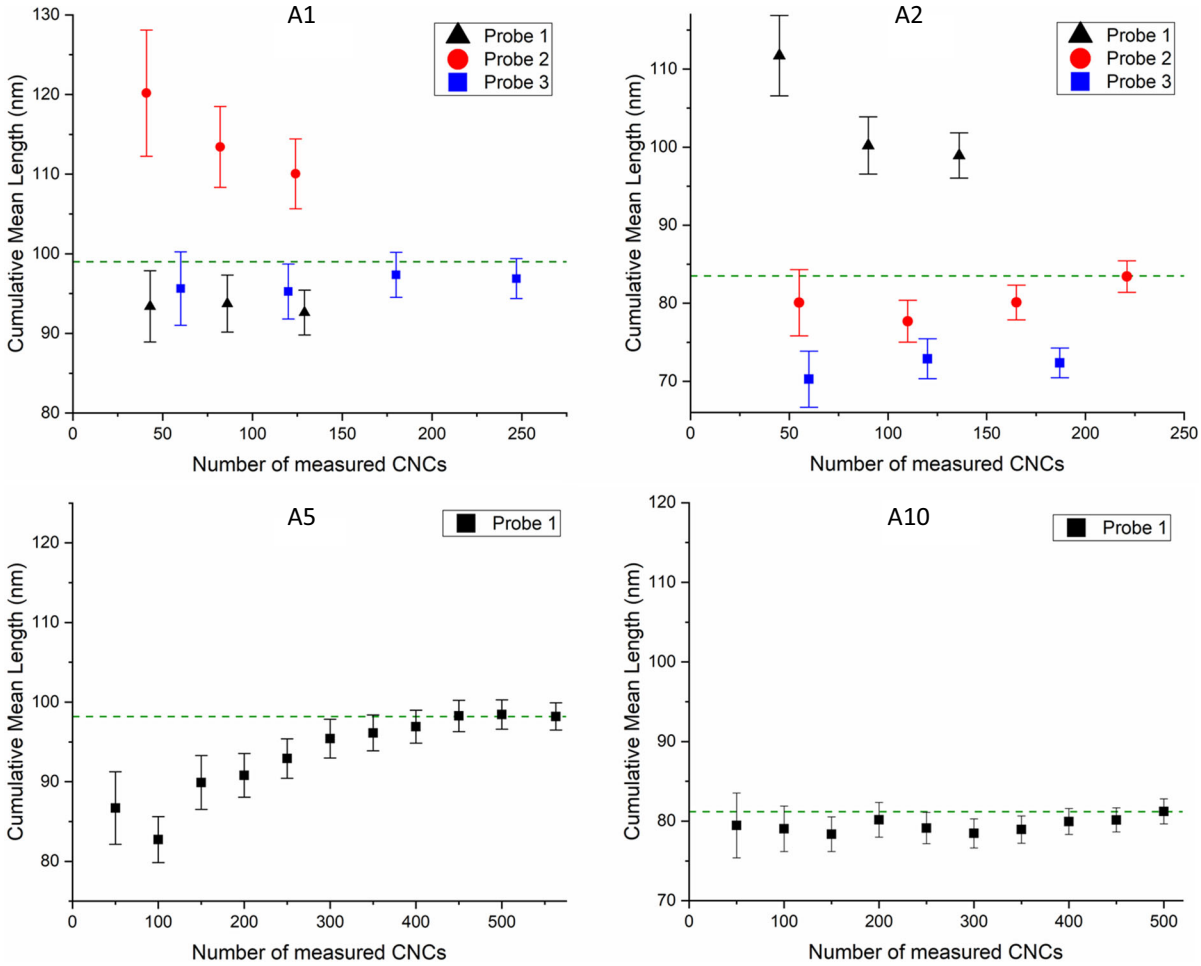

Fig. 3 Plots illustrating the mean CNC length as a function of the probe used and the number of particles analyzed. The cumulative mean for each probe used for selected laboratories is displayed in a different color/symbol with the standard error as an error bar; the dashed line provides the mean length for the entire data set for that laboratory. The representative examples show the effect of using multiple probes (A1, A2) and the evolution in mean length as a function of increased image acquisition for a single probe (A5, A10). Note that the y-axis covers a 50 nm range for all plots, although the origin is offset due to differences in the length range covered by the various data sets

et al. 2015; Grulke et al. 2017, 2018a, b; Petersen et al. 2019). The models and approaches utilized in these studies include normal, lognormal and Weibull distributions as well as discrete multinomial distributions and mixtures of Gaussian distributions.

We previously evaluated the particle size distributions for TEM data collected as part of this ILC (Meija et al. 2020) against more than 50 continuous probability distributions (Voncken et al. 2019). Probability density functions were fitted to data using the maximum likelihood method and the quality of each model was assessed by the Bayesian Information Criterion (BIC), which balances the simplicity of the model and the goodness of fit. Several distributions produced reasonable fits for the TEM data sets, the simplest of which are the lognormal and skew normal distributions. Based on the quality of fit to these 2 distributions for all 20 data sets, the skew normal distribution was selected for analysis of CNC size data since it fits the data very well and is relatively simple (3 parameters) and flexible (compatible with both positive and negative skew). This distribution has 3 parameters that measure central location (mean), scale (distribution width assessed as standard deviation) and a shape factor, α; the additional shape factor allows for either positive or negative skew in the particle size

distribution and should not be confused with the particle shape. By contrast to the lognormal distribution, skew normal has the advantage of becoming a normal distribution for data sets with no asymmetry. Therefore, the skew normal distribution is a suitable model for data sets that follow either normal or lognormal distributions, as well as those with a degree of asymmetry that is incompatible with either of the simpler distributions.

To facilitate comparison with the TEM results we employed a similar approach for analysis of the AFM data sets. As an example, Fig. S12 shows log–log cumulative probability plots for A1 length and height data along with fits to several different distributions. The skew normal distribution provides a better fit than the other three models for length data sets, and there are only minor differences between the various models for height. Fits to a skew normal distribution for AFM length and height are shown for several representative data sets in Fig. 4; the data sets were chosen to illustrate the variability in the distribution widths and asymmetries (as measured by the shape factor, α). The skew normal fits for all ten data sets for length, height and aspect ratio are shown in Fig. S4, S5 and S6, respectively, along with histograms for each data set. Table 1 summarizes mean, scale, and shape factors for length, height, and aspect ratio for each laboratory.

Consensus distributions, parameters, and uncertainty

The consensus distributions for the fitted parameters (Fig. 5) were obtained using the approach implemented in the TEM study in which all results were pooled together, an approach that makes the fewest number of assumptions (Meija et al. 2020). The statistical model is similar to the approach used by Montoro Bustos (Montoro Bustos et al. 2015), but with the use of skew normal distributions, rather than mixtures of Gaussian distributions, to model the individual data sets. This appears to be a reasonable choice since, as noted above, the skew normal distribution is appropriate for data sets that fit normal and lognormal distributions, as well as those with significant degrees of asymmetry. The skew normal consensus distribution was obtained by pooling the skew normal distributions for the individual laboratory results. An equal number of random samples ($N = 1000$) was drawn from each of the skew normal distributions and placed into the pool. In summary, the statistical model for the entire ILC study (for each measurand) is summarized by 3 parameters for the data from each laboratory as well as 3 additional parameters that describe the distribution of consensus values: the grand mean, scale, and shape.

The individual particle size distributions for the 10 laboratories for each of the 3 AFM measurands (height, length and aspect ratio) are shown in Fig. 5 and compared to the consensus distribution obtained using the above approach. The final consensus data for length, width, and aspect ratio with their associated uncertainties are summarized in Table 1; the uncertainties are obtained by fitting to the skew normal model. Overdispersion, t, values are also provided and indicate the presence of greater variability in the data sets than would be expected based on the statistical model used. The overdispersion values are all substantially larger than their uncertainties, indicating significant spread in the data sets as illustrated qualitatively by the histograms, quantile plots and fitted parameters in Table 1. The overdispersion values can be employed for assessment of the agreement between the individual laboratory means and the consensus value and identification of potential outliers.

Data comparisons

The skew normal fit parameters in Table 1 summarize the agreement between individual labs which is shown qualitatively in Fig. 2 and 5. Figure 6 displays the agreement between the length and height distributions for the various laboratories expressed as the overlap index, which is defined as the relative common area between two distributions. For height data, the overlap between pairs of data sets is high with only 4 values that are less than 0.75 and with the average overlap for a specific data set with all other data sets above 0.75. Data set A2 has the lowest overlap with other laboratories (3 values < 0.75); however, the mean for A2 is 0.54 nm lower than the consensus mean, which is less than twice the overdispersion and does not support considering this data set an outlier. The average overlap for A4 and A10 which used Peak Force imaging mode with low spring constant probes (facilitating imaging at low applied force) is high and their mean heights (3.4 and 3.5 nm, respectively) are close to the consensus value (3.4 nm, Table 1); this

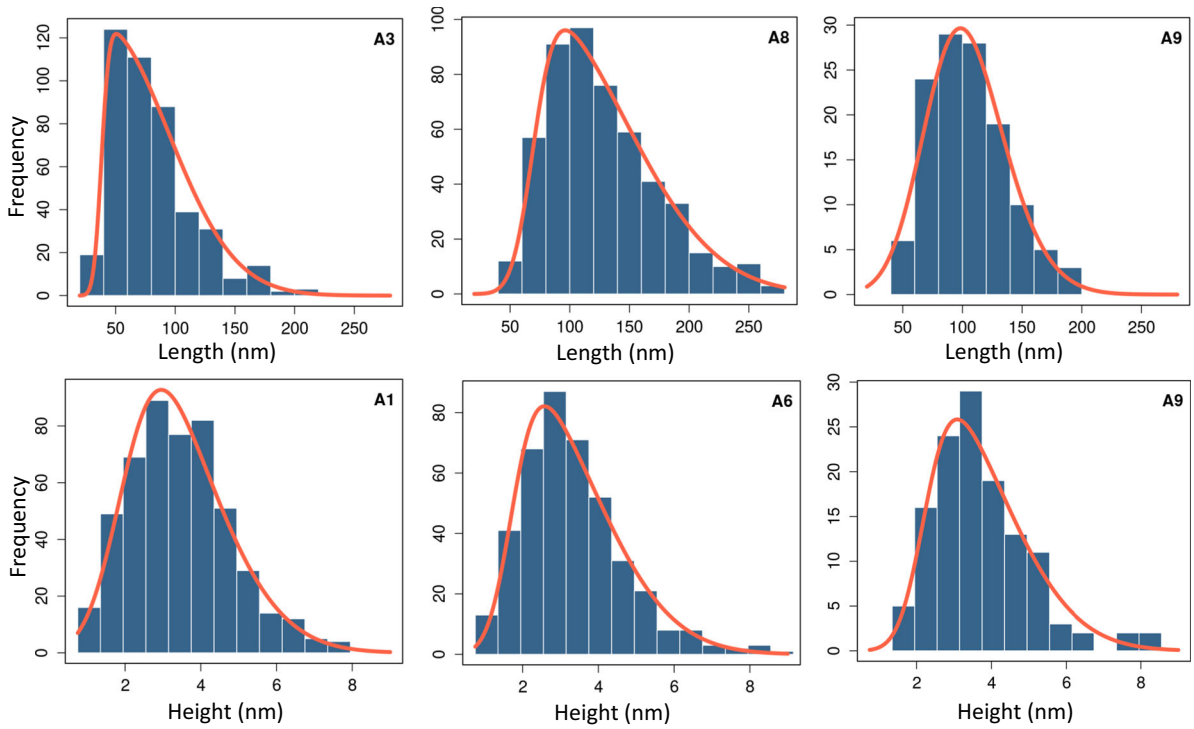

Fig. 4 Representative data sets showing histograms for AFM length and height and the fits to skew normal distributions (orange lines). The entire data set is used for fitting and the histograms allow a visual comparison of the data to the skew normal distribution

Table 1 Summary of skew normal fit parameters (distribution mean, standard deviation and shape factor) for individual data sets for each laboratory and the final consensus distribution for AFM length, height, and aspect ratio

Laboratory	Length			Height			Aspect ratio		
	Mean (nm)	Std dev (nm)	Shape, α	Mean (nm)	Std dev (nm)	Shape, α	Mean	Std dev	Shape, α
A1	99.7	40.0	7.6	3.4	1.4	2.5	32.2	12.7	7.1
A2	83.5	31.4	7.5	2.9	0.8	1.4	31.0	12.5	8.2
A3	82.5	33.9	10.9	3.7	1.0	1.6	22.8	7.8	6.5
A4	93.8	36.6	6.1	3.4	1.3	3.0	29.7	11.4	6.3
A5	98.6	40.0	8.0	3.7	1.1	3.7	27.6	10.4	5.7
A6	98.8	42.3	6.2	3.3	1.3	4.1	31.6	12.1	7.4
A7	79.4	29.9	7.5	3.1	1.2	3.4	27.7	9.5	5.7
A8	129.3	47.5	5.4	3.5	1.4	3.2	42.6	17.8	10.7
A9	103.7	34.1	1.5	3.7	1.3	3.6	31.0	13.4	3.3
A10	82.4	33.5	5.9	3.5	1.2	2.0	24.3	9.1	6.3
Consensus value (standard uncertainty)	94.5	39.6	6.4	3.44	1.21	2.7	30.3	12.8	6.8
	(0.4)	(0.3)	(0.3)	(0.01)	(0.01)	(0.1)	(0.1)	(0.1)	(0.2)
Overdispersion (uncertainty)	15.0			0.28			5.5		
	(0.6)			(0.02)			(0.2)		

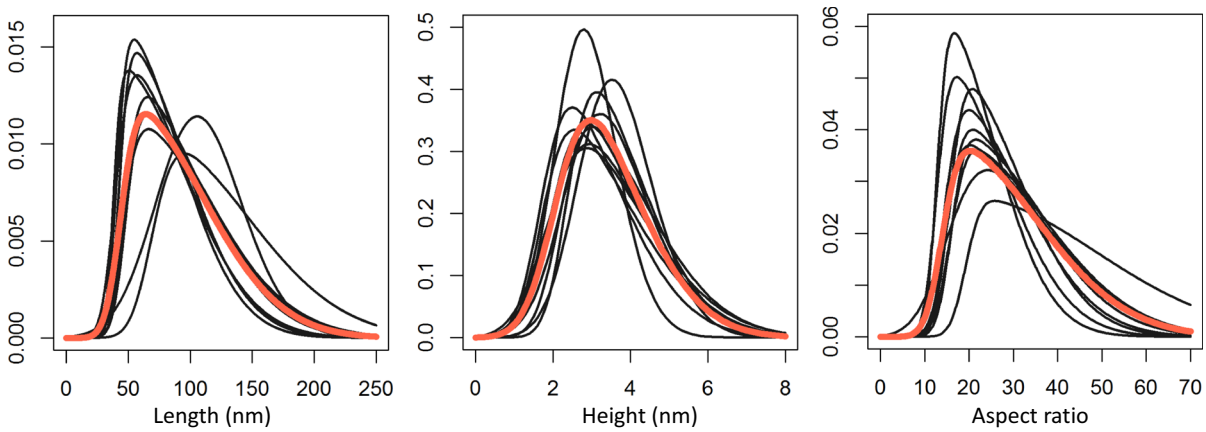

Fig. 5 Skew normal probability densities describing the individual laboratory results (black line) and the corresponding consensus distribution (orange line)

suggests that the variation in height across the 10 laboratories is unlikely to be due to reduction in CNC height by excessive applied force. The high overlap between labs and the low overdispersion value for the consensus height (0.28 ± 0.02 nm) indicate that the CNC height measurements are reproducible across different laboratories, instruments, probe types and samples. Factors such as the substrate used and the CNC charge, that may impact AFM height measurements do not contribute to variability in the ILC data since all samples were prepared using the same CNC reference material and the same protocol. The overdispersion for the consensus mean height (0.28 nm) is slightly larger than the probe to probe variation observed for individual data sets (Fig. S10) and similar to the change in mean height as function of imaging when a single probe is used (Fig. S11).

The overlap between data sets for length is lower than for height with $\sim$ 25% of the overlap index values < 0.75. Most of the low overlap values are for Lab A8 and, to a lesser extent, Lab A9. Lab A8 has the highest mean length with the largest distribution width (Table 1, mean, 129 nm and std dev, 47.5 nm). A possible explanation may be the automated imaging mode employed by this laboratory which resulted in changes in image quality throughout the data acquisition and less well-resolved CNCs. Note that the difference between the A8 mean length and the consensus mean is 2.3 times the overdispersion indicating that this data set is close to being an outlier. Interestingly, laboratory A9 analyzed the smallest number of particles (125 CNCs) and had the second largest mean (103.7 nm); this data set also had a population of shorter CNCs that was not observed for other data sets and fewer long CNCs. Based on the plots shown in Fig. S8 it appears that the small data set contributes to the lower overlap of A9 with other laboratories. Two labs with smaller tip radii (A4 and A10) have mean lengths that are similar to and lower than the consensus value, respectively, inconclusive as to whether the nominally smaller tip radius affects the measured CNC length. Only one lab (Lab A5) used a higher imaging resolution (0.98 nm/pixel) than the others, but there is no evidence that this has a significant impact as the mean and width of the length distribution are similar to the consensus value. All laboratories analyzed 1 μm × 1 μm images so the variation between laboratories is not due to changes in image size. It is interesting to note that the difference between probes used by an individual laboratory is in some cases similar to the overdispersion of the consensus mean (Table 1), indicating that this is a significant contributor to the variability between laboratories. The variations between laboratories observed in this study are similar to those observed in two other AFM ILCs of spherical nanoparticles with low polydispersity, although it is not stated whether the data was obtained with one or multiple probes (Meli et al. 2012; Lin et al. 2019). The present ILC was designed to minimize variability due to CNC dispersion and deposition on mica and it will be of interest to assess the impact this factor in future studies.

The AFM results can be compared to the TEM ILC results published separately (Meija et al. 2020). Both

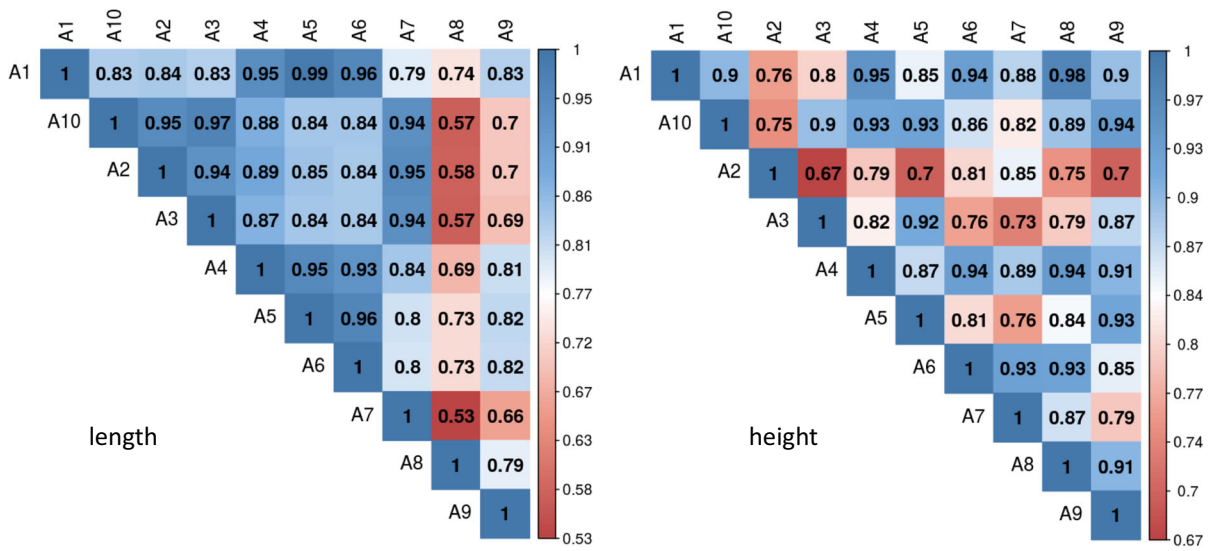

Fig. 6 Degree of overlap (overlap index) between skew normal distributions for AFM length and height for 10 participating laboratories

AFM and TEM data show similar levels of variability (as assessed by the uncertainty for the consensus parameters and the overdispersion values) between the 10 participating laboratories. In comparing the final consensus distributions, 2 observations stand out. First, the consensus distributions for length from the 2 methods are in excellent agreement with mean and standard deviation of 94.5 nm and 39.6 nm for AFM and 95.8 nm and 38.2 nm for TEM, respectively. The agreement between length measurements is in contrast to the original characterization data for CNCD-1, which was used to prepare the ILC samples. The original characterization study had reported a smaller AFM length (76 nm) compared to TEM (87 nm) (http://www.nrc.ca/crm; Brinkmann et al. 2016; Jakubek et al. 2018). Both length values are smaller than the final ILC consensus values, although still well within the range of the mean length values obtained by the ten laboratories. The ILC results indicate that, with a sufficiently large data set, AFM and TEM results are in excellent agreement, with a mean length of $\sim$ 95 nm. It is also worth noting that there are 2 participating labs that provided both AFM and TEM data sets for the ILC; the means for AFM and TEM for each laboratory differ by less than 2 nm, although the distribution widths vary by a larger amount. Comparison of the CNCD-1 size to literature data for other wood pulp-derived CNCs indicates that CNCD-1 has somewhat shorter particles, a result that can be attributed primarily to differences in hydrolysis conditions and processing (Moon et al. 2011; Reid et al. 2017; Foster et al. 2018). The more rigorous ILC protocol for identification of individual CNCs for analysis may also contribute to size differences.

The second observation is that the AFM and TEM ILC data (Meija et al. 2020) confirm the previous report of a TEM width that is approximately twice the AFM height (Jakubek et al. 2018) for CNCD-1. The consensus distributions have means and distribution widths of 7.7 nm and 2.2 nm for TEM width and 3.4 nm and 1.2 nm for AFM height. A number of data acquisition and analysis factors could contribute to this difference; these include TEM focusing conditions, poor TEM contrast, image resolution and analysis methods and AFM imaging force. However, the ILC consensus results are based on data from ten laboratories for both AFM and TEM making it unlikely that such factors are responsible for the large difference between height and width. One can therefore conclude either that the individual particles have an asymmetric cross-section and adsorb on the TEM grid with their larger side on the surface or that there is a fraction of laterally aggregated CNCs that cannot be distinguished as two particles by TEM.

The initial models for the elementary fibrils of plant-derived CNCs proposed an approximately symmetrical cross-section with a 6 $\times$ 6 array of polymer chains that were assembled during biosynthesis by an

enzyme complex with six-fold symmetry (Brown 1996; Moon et al. 2011). Individual fibrils were assigned a square geometry with cross-sectional dimensions that ranged between 3 and 5 nm, depending on the measurement method and the cellulose source (Hamad and Hu 2010; Jiang et al. 2010; Fernandes et al. 2011). Other studies have suggested variable numbers of polymer chains in the plant-based fibrils with diamond, parallelogram and hexagonal geometries for the fibril cross-section (Fernandes et al. 2011; Wang and Hong 2016). Nevertheless, the estimates for the cross-sectional dimensions of plant-derived fibrils fall within the range of 3–5 nm, with differences of 20–30% in the 2 cross-section dimensions. A recent AFM study of a fractionated CNCD-1 sample employed gold nanoparticles as an internal calibration standard to determine the AFM tip radius (Chen et al. 2020a, b). The tip radius was used to correct measured CNC widths for tip-particle convolution effects, allowing the measurement of width and height for the same particles for a fractionated CNCD-1 sample with very few clustered particles. This demonstrated that some particles have cross-sections with approximately equal dimensions for the 2 axes, whereas others have long axes that are between 2 and 3.5 times larger than the short axis. The dimensions of the symmetric particles are consistent with the expected dimensions for the elementary fibrils of plant derived CNCs. They are also consistent with AFM measurements of elementary fibrils in plant cell walls (Ding et al. 2012; Zhang et al. 2015). Interestingly the latter studies also visualized lateral aggregation of fibrils. Both the presence of particles comprised of multiple crystallites and particle aggregation have been reported in other studies (Elazzouzi-Hafraoui et al. 2008; Kaushik et al. 2014; Cherhal et al. 2015; Uhlig et al. 2016). Based on the above considerations, the ILC TEM width measurements may be attributed to a combination of aggregation of individual particles that is not readily distinguishable by TEM and the presence of multiple laterally assembled crystallites in some CNC particles.

Conclusions

AFM length and height data sets were obtained from 10 laboratories participating in the ILC. There is considerable variation in the overall central location, distribution width and asymmetry for the various data sets, particularly for length. This variability has prompted an analysis approach that involves fitting the data to a skew normal distribution which includes an additional shape factor that accommodates the variable skew in the data sets. The skew normal distribution has the advantage of becoming equivalent to a normal distribution for cases where the shape factor is equal to zero. ILC consensus values were then obtained by modelling the variation between the individual laboratories as a skew normal distribution.

The final consensus values for length are in excellent agreement with the TEM results obtained as part of the same ILC. The agreement between individual height data sets is reasonably high as judged by the overlap index plots (Fig. 6). It appears that a repeatable data set for an individual laboratory can be obtained with considerably less than the 500 data points requested for the ILC. However, there is a wider spread of data for length and it is difficult to separate effects of tip properties, number of CNCs analyzed and possibly other operating parameters that are not captured in this study. The use of multiple probes and/or deterioration of the probe properties as a function of increased use are significant contributors to the variability between laboratories, particularly for length. Based on image analysis tests in the first phase of the ILC, analyst subjectivity in selection and size measurements for individual particles is a minor contributor to the variability in the determination of CNC length. Finally, the combined AFM and TEM results obtained in this ILC indicate the factors that should be considered to obtain reliable particle size data and to make comparisons between different sources of CNCs for quality control purposes. Although measurements such as these are unlikely to be undertaken frequently by CNC producers, they serve as a useful study against which other more routine measurements may be benchmarked. Since a variety of instruments and AFM probes were used by the ILC participants, it is likely that the observed variation in data is typical of that expected over a wider range of laboratories. Future studies to assess the impact of sample preparation in multiple laboratories, the development of automated image analysis methods and better control over AFM probe properties would be beneficial.

Acknowledgments We thank Dr. Jeff Fagan, NIST for useful advice while planning this ILC. Funding to the NRC from Natural Resources Canada's Forestry Innovation Program for CNC standardization work is gratefully acknowledged. Funding from the Australian Research Centre-Industry Transformation Research Hub; Processing Advanced Lignocellulosics (PALS) [Grant Number IH170100020] to WB is gratefully acknowledged.

Compliance with ethical standards

Conflict of interest The authors declare that they have no conflicts of interest.

Human or animal rights This article does not contain any studies with human participants or animals performed by any of the authors.

Informed consent Informed consent was obtained from all individual participants included in the study.

References

Beck-Candanedo S, Roman M, Gray DG (2005) Effect of reaction conditions on the properties and behavior of wood cellulose nanocrystal suspensions. Biomacromol 6:1048–1054. https://doi.org/10.1021/bm049300p

Brinkmann A, Chen M, Couillard M, Jakubek ZJ, Leng T, Johnston LJ (2016) Correlating cellulose nanocrystal particle size and surface area. Langmuir 32:6105–6114. https://doi.org/10.1021/acs.langmuir.6b01376

Brito BSL, Pereira FV, Putaux J-L, Jean B (2012) Preparation, morphology and structure of cellulose nanocrystals from bamboo fibers. Cellulose 19:1527–1536

Brown RM (1996) The biosynthesis of cellulose. Pure Appl Chem A33:1345–1373. https://doi.org/10.1080/10601329608014912

Chen M, Parot J, Hackley VA, Zou S, Johnston LJ (2020) AFM characterization of cellulose nanocrystal height and width using internal calibration standards. Cellulose submitted.

Chen M, Parot J, Mukherjee A, Couillard M, Zou S, Hackley VA, Johnston LJ (2020) Characterization of size and aggregation for cellulose nanocrystal dispersions separated by asymmetrical-flow field-flow fractionation. Cellul 27:2015–2028. https://doi.org/10.1007/s10570-019-02909-9(0123456

Cherhal F, Cousin F, Capron I (2015) Influence of charge density and ionic strength on the aggregation process of cellulose nanocrystals in aqueous suspension, as revealed by small-angle neutron scattering. Langmuir 31:5596–5602. https://doi.org/10.1021/acs.langmuir.5b00851

Delvallee A, Feltin N, Ducourtieux S, Trabelsi M, Hochepied JF (2016) Toward an uncertainty budget for measuring nanoparticles by AFM. Metrologia. https://doi.org/10.1088/0026-1394/53/1/41

Delvallée A, Feltin N, Ducourtieux S, Trabelsi M, Hochepied JF (2015) Direct comparison of AFM and SEM measurements on the same set of nanoparticles. Meas Sci Tech. https://doi.org/10.1088/0957-0233/26/8/085601

Ding S-Y, Liu Y-S, Zeng Y, Himmel ME, Baker JO, Bayer EA (2012) How does plant cell wall nanoscale architecture correlate with enzymatic digestibility? Sci 338:1055–1060. https://doi.org/10.1126/science.1227491

Elazzouzi-Hafraoui S, Nishiyama Y, Putaux J-L, Heux L, Dubreuil F, Rochas C (2008) The shape and size distribution of crystalline nanoparticles prepared by acid hydrolysis of native cellulose. Biomacromolecules. https://doi.org/10.1021/bm700769p

Fernandes AN, Thomas LH, Altaner CM, Callow P, Forsyth VT, Apperley DC, Kennedy CJ, Jarvish MC (2011) Nanostructure of cellulose microfibrils in spruce wood. Proc Natl Acad Sci. https://doi.org/10.1073/pnas.1108942108

Foster EJ, Moon RJ, Agarwal UP, Bortner MJ, Bras J, Camarero-Espinosa S, Chen KJ, Clift MJD, Cranston ED, Eichhorn SJ, Fox DM, Hamad WY, Heux L, Jean B, Korey M, Nieh W, Ong KJ, Reid MS, Renneckar S, Roberts R, Shatkin JA, Simonsen J, Stinson-Bagby K, Wanasekara N, Youngblood J (2018) Current characterization methods for cellulose nanomaterials. Chem Soc Rev 47:2609–2679. https://doi.org/10.1039/C6CS00895J

Grishkewich N, Mohammed N, Tang J, Tam C (2017) Recent advances in the application of cellulose nanocrystals. Curr Opin Colloid Inter Sci 29:32–45. https://doi.org/10.1016/j.cocis.2017.01.005

Grulke EA, Rice SB, Xiong J, Yamamoto K, Yoon TH, Thomson K, Saffaripour M, Smallwood GJ, Lambert JW, Stromberg AJ, Macy R, Briot NJ, Qian D (2018a) Size and shape distributions of carbon black aggregates by transmission electron microscopy. Carbon 130:822–833. https://doi.org/10.1016/j.carbon.2018.01.030

Grulke EA, Wu X, Ji Y, Buhr E, Yamamoto K, Song NW, Stefaniak AB, Schwegler-Berry D, Burchett WW, Lambert J, Stromberg AJ (2018b) Differentiating gold nanorod samples using particle size and shape distributions from transmission electron microscope images. Metrologia 55:254–267. https://doi.org/10.1088/1681-7575/aaa368

Grulke EA, Yamamoto K, Kumagi K, Hausler I, Osterle W, Ortel E, Hodoroaba V-D, Brown SC, Chan C, Zheng J, Yamamoto K, Yashiki K, Song NW, Kim YH, Stefaniak AB, Schwegler-Berry D, Coleman VA, Jamting AK, Hermann J, Arakawa T, Burchett WW, Lambert JW, Stromberg AJ (2017) Size and shape distributions of primary crystallites in titania aggregates. Adv Powder Tech 28:1647–1659. https://doi.org/10.1016/j.apt.2017.03.027

Hamad WY, Hu TQ (2010) Structure-property-yield inter-relationships in nanocrystalline cellulose extraction. Can J Chem Eng 88:392–402. https://doi.org/10.1002/cjce.20298

Jakubek ZJ, Chen M, Couillard M, Leng T, Liu L, Zou S, Baxa U, Clogston JD, Hamad W, Johnston LJ (2018) Characterization challenges for a cellulose nanocrystal reference material: dispersion and particle size distributions. J Nanopart Res 20:98. https://doi.org/10.1007/s10570-019-02909-9

Jiang F, Esker AR, Roman M (2010) Acid-catalyzed and solvolytic desulfation of H_2SO_4-hydrolyzed cellulose nanocrystals. Langmuir 26:17919–17925. https://doi.org/10.1021/la1028405

Johnston LJ, Jakubek ZJ, Beck S, Araki J, Cranston ED, Danumah C, Fox D, Li H, Wang J, Mester Z, Moores A, Murphy K, Rabb SA, Rudie A, Stephan C, (2018) Determination of sulfur and sulfate half-ester content in cellulose nanocrystals: an interlaboratory comparison. Metrologia 55:872–882. https://doi.org/10.1088/1681-7575/aaeb60

Kaushik M, Chen WC, van de Ven TGM, Moore A (2014) An improved methodology for imaging cellulose nanocrystals by transmission electron microscopy. Nordic Pulp Paper Res J 29:77–84. https://doi.org/10.3183/npprj-2014-29-01-p077-084

Kaushik M, Fraschini C, Chauve G, Putaux J-L, Moores A (2015) Transmission electron microscopy for the characterization of cellulose nanocrystals. In: Maaz K (ed) The transmission electron microscope-theory and applications. Intech. https://doi.org/10.5772/59457

Kestens V, Roebben G, Herrmann J, Jamting A, Coleman V, Minelli C, Clifford C, De Temmerman P-J, Mast J, Junjie L, Babick F, Colfen H, Emons H (2016) Challenges in the size analysis of a silica nanoparticle mixture as candidate certified reference material. J Nanopart Res 18:171. https://doi.org/10.1007/s11051-016-3474-2

Kiss LB, Soderlund J, Niklasson GA, Granqvist CG (1999) New approach to the origin of lognormal size distributions of nanoparticles. Nanotechnol 10:25–28. https://doi.org/10.1088/0957-4484/10/1/006

Klemm D, Kramer F, Moritz S, Lindstrom T, Ankerfors M, Gray D, Dorris A (2011) Nanocelluloses: a new family of nature-based materials. Angew Chem Int Ed Engl 50:5438–5466. https://doi.org/10.1002/anie.201001273

Korolovych VF, Cherpak V, Nepal D, Ng A, Shaikh NR, Grant A, Xiong R, Bunning TJ, Tsukruk VV (2018) Cellulose nanocrystals with different morphologies and chiral properties. Polym 145:334–347. https://doi.org/10.1016/j.polymer.2018.04.064

Lahiji RR, Xu X, Reifenberger R, Raman A, Rudie A, Moon RJ (2010) Atomic force microscopy characterization of cellulose nanocrystals. Langmuir 26:4480–4488. https://doi.org/10.1021/la903111j

Lin H-L, Fu W-E, Weng H-F, Misumi I, Sugawara K, Gonda S, Takahashi K, Takahata K, Ehara K, Takatsuji T, Fujimoto T, Salas J, Dirschel K, GarnÃ¦s KJ, Damasceno J, de Oliveira JCV, Emanuele E, Picotto GB, Kim CS, Cho SJ, Motzkus C, Meli F, Gao S, Shi Y, Liu J, Jamting K, Catchpoole HJ, Lawn MA, Herrmann J, Coleman VA, Adlem L, Kruger OA, Buajarern J, Buhr E, Danzebrink H-U, Krumrey M, Bosse H (2019) Nanoparticle characterization-supplementary comparison on nanoparticle size. Metrologia 56:04004. https://doi.org/10.1088/0026-1394/56/1A/04004

Mattos BD, Tardy BL, Rojas OJ (2019) Accounting for substrate interactions in the measurement of the dimensions of cellulose nanofibrils. Biomacromol 20:2657–2665. https://doi.org/10.1021/acs.biomac.9b00432

Meija J, Bushell M, Couillard M, Beck S, Bonevich J, Cui K, Foster J, Will J, Fox D, Cho W, Heidelmann M, Park BC, Park YC, Ren L, Xu L, Stefaniak A, Knepp AK, Theissmann R, Purwin H, Wang Z, de Val N, Johnston LJ (2020) Particle size distributions for cellulose nanocrystals measured by transmission electron microscopy: an interlaboratory comparison. Anal Chem 92:13434–13442. https://doi.org/10.1021/acs.analchem.0c02805

Meli F, Klein T, Buhr E, Frase CG, Gleber G, Krumrey M, Duta A, Duta S, Korpelainen V, Bellotti R, Picotto GB, Boyd RD, Cuenat A (2012) Traceable size determination of nanoparticles, a comparison among European Metrology Institutes. Meas Sci Tech 23:125005. https://doi.org/10.1088/0957-0233/23/12/125005

Meng Y, Wu Q, Young TM, Huang B, Wang S, Li Y (2017) Analyzing three-dimensional structure and geometrical shape of individual cellulose nanocrystal from switchgrass. Polym Compos. https://doi.org/10.1002/pc.23819

Mokhena TC, John MJ (2020) Cellulose nanomaterials: new generation materials for solving global issues. Cellulose 27:1149–1194. https://doi.org/10.1007/s10570-019-02889-w

Mondal S (2017) Preparation, properties and applications of nanocellulosic materials. Carbohy Poly 163:301–316. https://doi.org/10.1016/j.carbpol.2016.12.050

Montoro Bustos AR, Petersen EJ, Possolo A, Winchester MR (2015) Post hoc interlaboratory comparison of single particle ICP-MS size measurements of NIST gold nanoparticle reference materials. Anal Chem 87:8809–8817. https://doi.org/10.1021/acs.analchem.5b01741

Moon RJ, Martini A, Nairn J, Simonsen J, Youngblood J (2011) Cellulose nanomaterials review: structure, properties and nanocomposites. Chem Soc Rev 40:3941–3994. https://doi.org/10.1039/C0CS00108B

Moon RJ, Pohler T, Tammelin T (2014) Microscopic characterization of nanofibers and nanocrystals handbook of green materials. K Oksman, AP Mathew, A Bismarck, O Rojas, M Sain. Singapore, World Scientific, 1: 159–180, ISBN-13 : 978–9814566452

Ogawa Y, Putaux J-L (2019) Transmission electron microscopy of cellulose. part 2: technical and practical aspects. Cellulose 26:17–34. https://doi.org/10.1007/s10570-018-2075-x

Petersen EJ, Montoro Bustos AR, Toman B, Johnson ME, Ellefson M, Caceres GC, Neuer AL, Chan Q, Kemling JW, Mader B, Murphy K, Roesslein M (2019) Determining what really counts: modeling and measuring nanoparticle number concentrations. Environ Sci: Nano 6:2876–2896. https://doi.org/10.1039/C9EN00462A

Postek MT, Vladar A, Dagata J, Farkas N, Ming B, Wagner R, Raman A, Moon RJ, Sabo R, Wegner TH, Beecher J (2011) Development of the metrology and imaging of cellulose nanocrystals. Meas Sci Tech 22:024005. https://doi.org/10.1088/0957-0233/22/2/024005

Reid MS, Villalobos M, Cranston ED (2017) Benchmarking cellulose nanocrystals: from the laboratory to industrial production. Langmuir 33:1583–1598. https://doi.org/10.1021/acs.langmuir.6b03765

Schütz C, Van Rie J, Eyley S, Gençer A, van Gorp H, Rosenfeldt S, Kang K, Thielemans W (2018) Effect of source on the properties and behavior of cellulose nanocrystal suspensions. ACS Sustain Chem Eng 6:8317–8324. https://doi.org/10.1021/acssuschemeng.8b00334

Shatkin JA, Kim B (2015) Cellulose nanomaterials: life cycle risk assessment and environmental health and safety roadmap. Environ Sci: Nano 2:477–499. https://doi.org/10.1039/C5EN00059A

Shatkin JA, Wegner TH, Bilek EM, Cowie J (2014) Market projections of cellulose nanomaterial-enabled products-part 1: applications. TAPPI J 13:9–16. https://doi.org/10.32964/TJ13.5.9

Stinson-Bagby KL, Roberts R, Foster EJ (2018) Effective cellulose nanocrystal imaging using transmission electron microscopy. Carbohy Poly 186:429–438. https://doi.org/10.1016/j.carbpol.2018.01.054

Uhlig M, Fall A, Wellert S, Lehmann M, Prévost S, Wågberg L, von Klitzing R, Nyström G (2016) Two-dimensional aggregation and semidilute ordering in cellulose nanocrystals. Langmuir 32:442–450. https://doi.org/10.1021/acs.langmuir.5b04008

Usov I, Mezzenga R (2015) FiberApp: an open source software for tracking and analyzing polymers, filaments, biomacromolecules and fibrous objects. Macromol 48:1269–1280. https://doi.org/10.1021/ma502264c

Usov I, Nystrom G, Adamcik J, Handschin S, Schutz C, Fall A, Bergstrom L, Mezzenga R (2015) Understanding nanocellulose chirality and structure-properties relationship at the single fibril level. Nat Comm 6:7564. https://doi.org/10.1038/ncomms8564

Voncken L, Albers CJ, Timmerman ME (2019) Model selection in continuous test norming with GAMLSS. Assess 26:1329–1346. https://doi.org/10.1177/1073191117715113

Wang T, Hong M (2016) Solid-state NMR investigations of cellulose structure and interactions with matrix polysaccharides in plant primary cell walls. J Exp Botany 67:503–514. https://doi.org/10.1093/jxb/erv416

Zhang T, Zheng Y, Cosgrove DJ (2015) Spatial organization of cellulose microfibrils and matrix polysaccharides in primary plant cell walls as imaged by multichannel atomic force microscopy. Plant J 85:179–192. https://doi.org/10.1111/tpj.13102